Chapter 8

Experimental Testing of a 2d MFI Algorithm

8.1 Introduction

The previous chapters have dealt with the development and testing of a moving force identification algorithm based on first order Tikhonov regularisation and dynamic programming. Whilst numerical testing is useful for the initial validation of any inverse problem, the method is also tested experimentally here to assess the validity of the inverse method.

This chapter describes the experimental testing carried out on the Vransko Bridge in Slovenia. The testing carried out was collaboration between University College Dublin (UCD) and the Slovenian National Building and Civil Engineering Institute (ZAG) and their subcontractors. A simply supported bridge of beam and slab construction was chosen as it is deemed to be of a suitable type for the testing of the MFI algorithm. The strain transducers and data acquisition system were both provided and installed by the personnel of ZAG. The installation and testing was carried out between 24th September 2006 and 1st October 2006.

8.2 Vransko Bridge Slovenia

The Vransko Bridge is located approximately 10km south of the Slovenian capital, Ljubljana, see figure 8.1. The bridge is 24.8m between the centre line of the bearings with a total span of 26 m. It has two same-direction lanes of traffic with a hard shoulder. The bridge has no skew and is of beam and slab construction. Figure 8.2 shows an elevation from the upstream side and figure 8.3 shows the bridge supports and the underside. The bridge was selected as it was deemed to be a good representation of a medium span orthotropic deck. The slab is constructed from concrete and has a layer of asphalt on top. The slab is supported by five concrete longitudinal beams, and two concrete diaphragm beams, located in the transverse direction over the supports. The geometric properties are taken from both on-site measurements and engineering drawings provided by ZAG. The elevation and cross section are shown in figures 8.4 and 8.5 respectively. There is a 2.5% camber across the deck and there are also a run on slab, see figure 8.5, which could effect the bridge response.

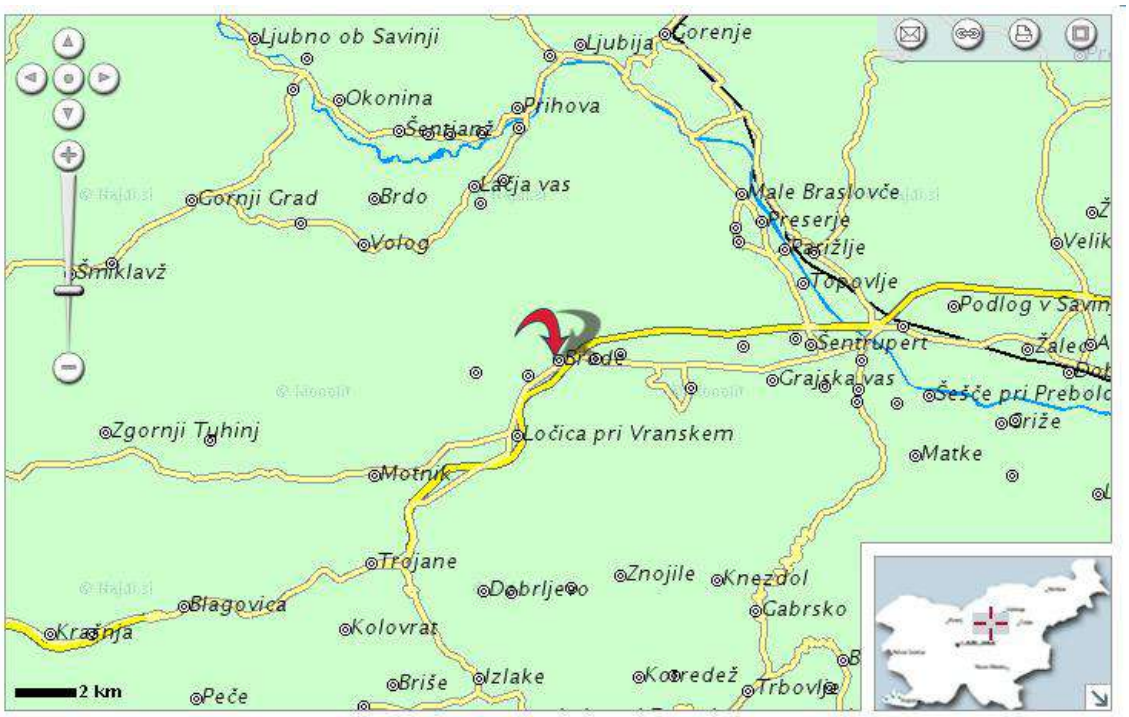

Figure 8.1 – Location of Vransko bridge indicated by red arrow

Figure 8.2 – Elevation of Vransko Bridge from upstream.

(a) - Bridge supported on bearings

(b) – Underside of bridge showing longitudinal beams

Figures 8.3 – Support conditions and underside of bridge

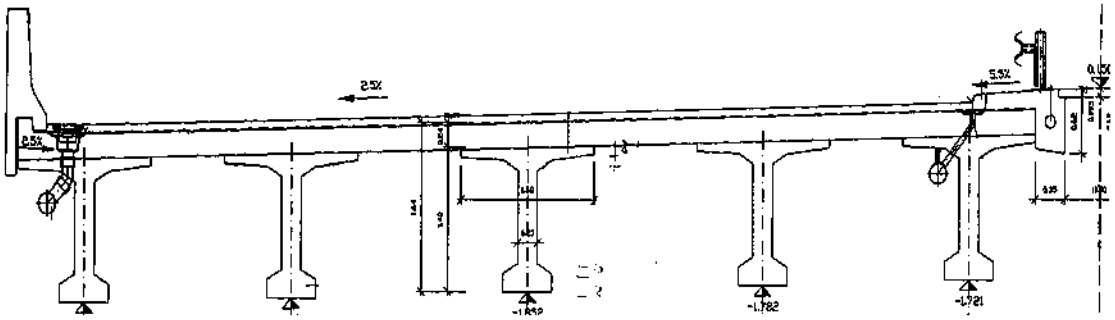

Figure 8.4 – Bridge cross section

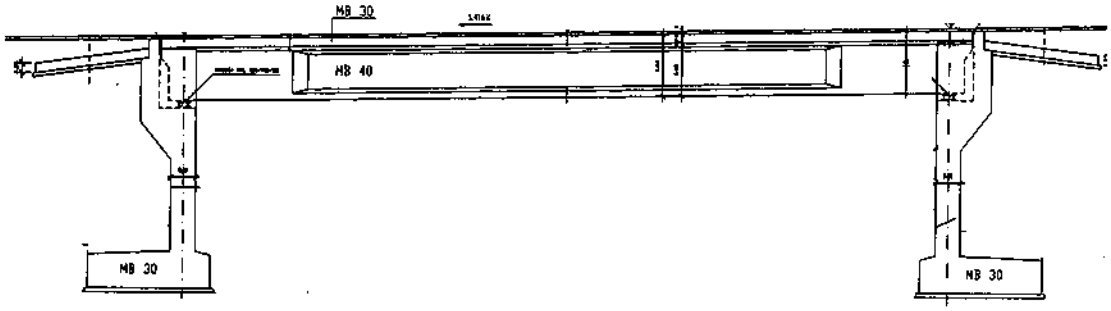

Figure 8.5 – Bridge elevation

8.3 Instrumentation and Data Acquisition

The bridge is instrumented with strain transducers to record the strain, and strain transducers at the quarter points for axle detection. The instrumentation and the installation of the data acquisition equipment was carried out by ZAG. In total, nineteen strain transducers were installed, 15 on the soffits of the beams and 4 on the soffit of the slab. Figure 8.6 shows a photograph of one of the strain transducers bolted to the soffit of one of the beams. The location of the strain transducers is shown in schematic form in figure 8.7.

Figure 8.6 – Strain transducer

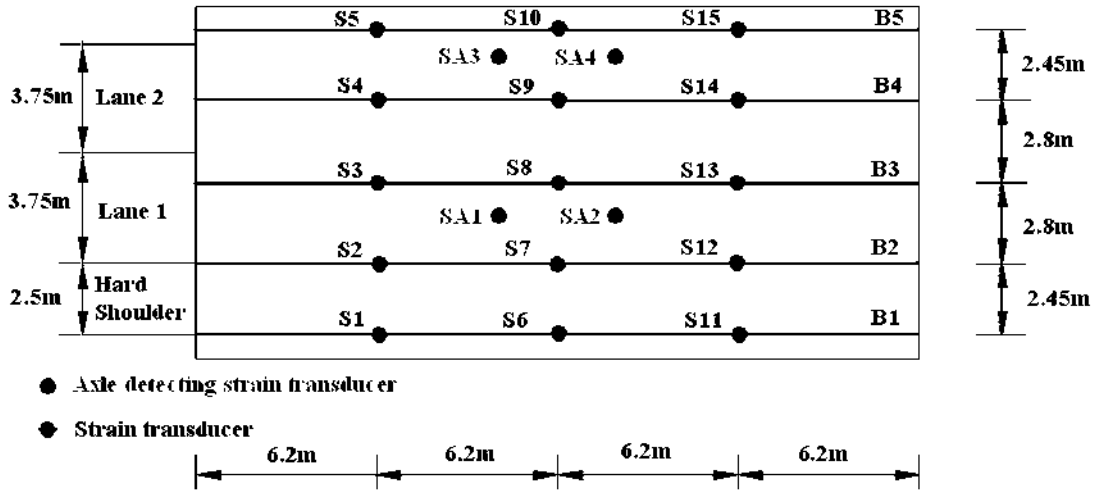

Figure 8.7 – Plan of deck, showing positions and number of the strain transducers and location and numbers of the beams.

The axle detectors, shown in schematic form in figure 8.7, give information on the vehicle velocity, the number of axles and the axle spacing. In conventional B-WIM systems, axle detectors are in the form of electrical tape switches or pneumatic tubes located at the entrance and exit of the bridge. However in this experiment the method of axle detection is that employed and developed by the ZAG institute. Strain transducers labelled SA1 to SA4 in figure 8.7, are installed at 45 degrees to the longitudinal on the soffit of the slab. When an axle crosses one of these sensors there is a very sharp spike in the magnitude of the strain response. These spikes can be used to calculate the vehicle velocity, number of axles and the axle spacing.

Figure 8.8 shows typical axle detector data for a 3-axle truck travelling in lane one. This figure shows the vehicle crossing the axle detecting strain transducers SA1 and SA2, which are spaced 4m apart; in both cases there are three distinct spikes in the response from these sensors representing the three axles of the truck. As the sampling rate is known and the distance between the axle detectors is known, the velocity and axle spacing can then be calculated from the response.

The data acquisition was carried out using a system developed by ZAG and hardware built by the Cestel Company. The scanning frequency of the data acquisition system is 512Hz; the data was recorded on a laptop using a program developed by ZAG (SiWIM). Figure 8.9 shows a photograph of the data acquisition system stored under the bridge.

Unfortunately static testing of the bridge was not possible, as the bridge is an in-service highway bridge, with upwards of 3000 trucks a day. Prior to this, the strain transducers were calibrated in ZAG's laboratory, and the only information available is that 1-volt is approximately 19.5×10^{-6} strain. The author acknowledges that these are not ideal conditions for the testing of the MFI algorithm. However the calibration of the strain transducers is not the only unknown in the experimental testing program. The exact properties of the bridge are not known, the material properties as specified by the design are known, but these could be quite different to the actual material properties of the in-service bridge. The Youngs modulus of the concrete in the beams and the slab, the exact depth of the slab and the interaction of the slab and the beams are all unknown.

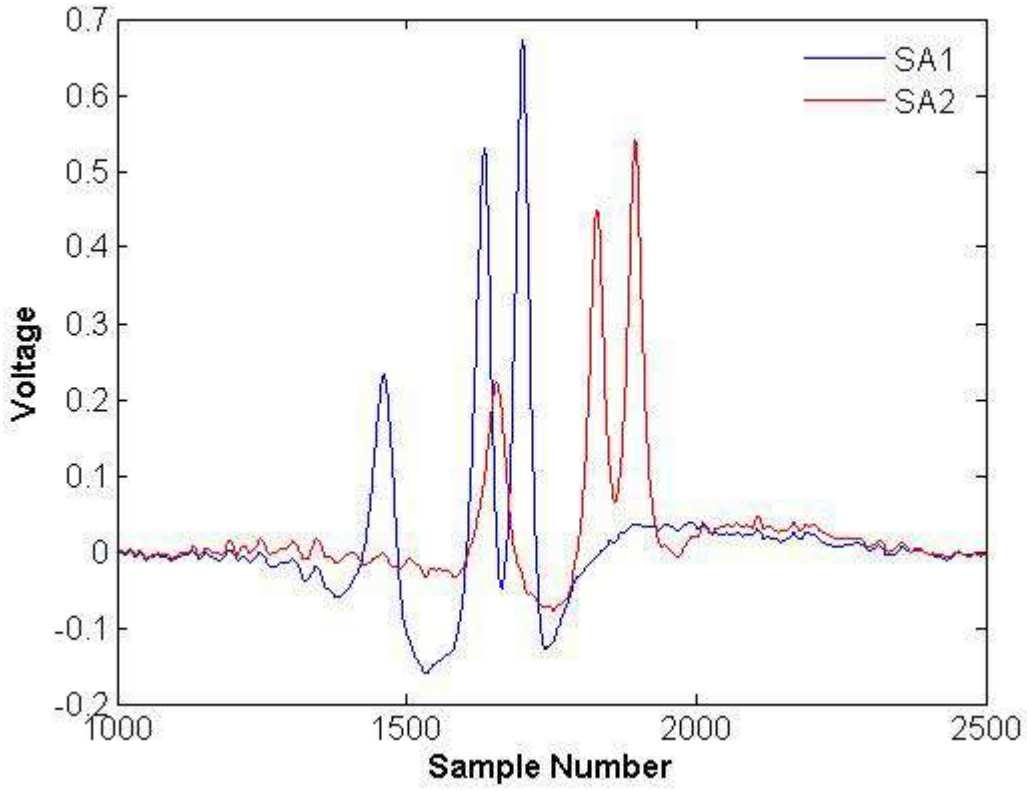

Figure 8.8 – Axle detector data

Figure 8.9 – Data acquisition system

8.4 Frequency Analysis

Frequency analysis was carried out to determine the natural frequencies of the bridge. The strain transducers at quarter, mid and three quarter span were used in the analysis. The signals are taken after the vehicle has traversed the bridge, and it is in free vibration. The frequency analysis was carried out using the FFT function in Matlab. In total, modal analysis was carried out on 35 different signals from 6 different events. Figure 8.10 shows typical FFT results for two different signals. The first five natural frequencies of the bridge were calculated from an average of all the signals analysed see table 8.1. This table shows the event number and the strain transducer as numbered in figure 8.7. The frequencies are ordered from smallest to largest for each sensor analysed and in many cases certain frequencies are not detected. The bridge-damping factor was calculated by ZAG to be approximately 1% for the first natural frequency.

		Mode					
Event	**Sensor**	**1**	**2**	**3**	**4**	**5**	**6**
1	S1	5.11		9.7	15.0		
	S2	5.11			16.5		
	S3	5.11		9.7	16.6	21.8	
	S4	5.11					
	S5	5.11	5.9				
	S6	5.11	6.9	9.7			
	S7	5.11	6.9	9.7			
	S8	5.11					
	S9	5.11					
	S10	5.11					
	S11	5.11		9.7			
	S12	5.11					
	S13	5.11		9.7			
2	S1	5.11			16.3		
	S2	5.11			16.3		
	S3	5.11		10.2	16.3		
	S4	5.11			16.3		
	S5	5.11			16.3		
	S6	5.11			16.3		
3	S1	5.11	6.2	9.5	15.5	21.5	24.0
	S2	5.11	6.5		15.8		24.8
	S3	5.11		9.5		21.5	
	S4	5.11		9.5		19.0	
	S5	5.11	6.6	9.5	16.0	19.5	
	S6	5.11	6.1		15.0		
4	S1	5.11			16.6		25.0
	S2	5.11		11.9	16.2		24.5
	S3	5.11			16.2		24.7
	S8	5.11			16.5		24.7
	S10	5.11			16.5		24.7
5	S1	5.11	6.6	10.2			
	S3	5.11	6.6	9.7			
	S5	5.11	6.6				
6	S5	5.11					
	S6	5.11	6.6	10.2			
	S8	5.11	6.6		16.2	20.0	
Average		**5.11**	**6.50**	**9.89**	**16.12**	**20.55**	**24.62**

Table 8.1 – Calculated frequencies for the 6 events

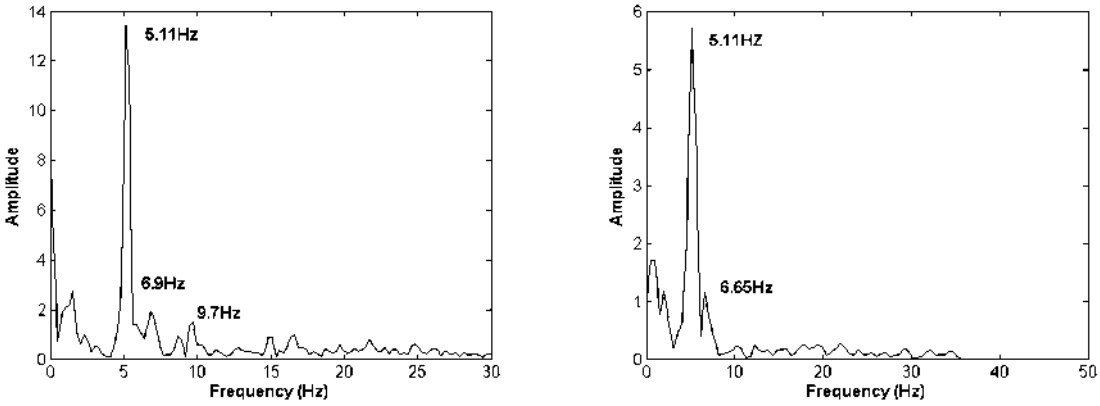

(a) – Frequency Response of event 1, S6 **(b) –** Frequency response of event 5, S5

Figure 8.10 – Fast Fourrier transform of two different signals

Mode	Frequency (Hz)
1	5.11
2	6.50
3	9.89
4	16.12
5	20.55
6	24.62

Table 8.2 – First six measured natural frequencies of the Vransko Bridge

8.5 Test Truck and Trial Details

A pre-weighed three-axle truck was used during testing. The truck is a rigid three-axle vehicle with steel suspension. The truck axles were weighed on site using portable weighing mats. Figure 8.11 shows photographs of the truck and the pressure cells. The truck was fully loaded with sand, and had static axle weights of 74.5kN, 100kN and 100kN; figure 8.12 shows the axle configuration as measured on site.

(a) –Test truck **(b)** – Static weighing

Figure 8.11 - Test truck

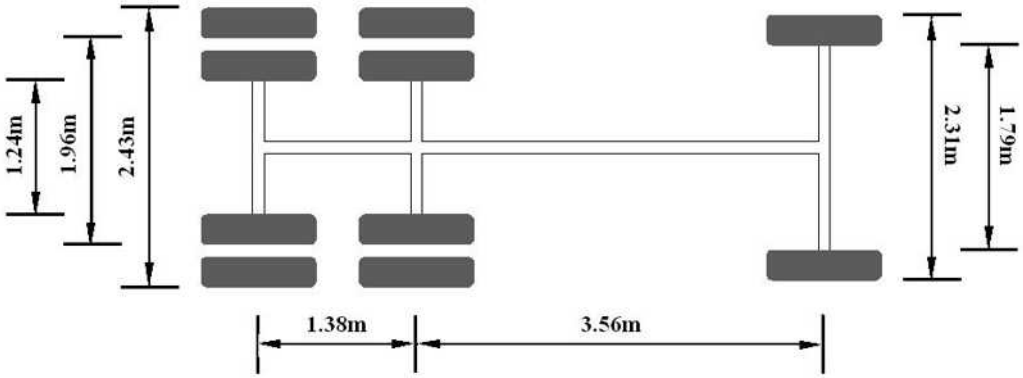

Figure 8.12 – Axle configuration

Experimental testing was carried out with the test truck on 26th of September 2006. The bridge receives a large volume of traffic per day. This coupled with a turnaround time of twenty minutes for runs of the truck, meant that in total only 14 single vehicle events were obtained. The data recorded for each event was the strain for each of the sensors and the voltage from the axle detectors; figure 8.13 shows typical strain records from the test vehicle. It should also be noted that the program SiWIM used to collect the data utilises a digital filter on the recorded data. As no information was provided on the nature of the filter, both the raw and filtered data were recorded for some of the test runs. It can also be seen from figure 8.14 that the magnitude of the response at three quarter span is only a fraction of that recorded at quarter span. This is due to the amplification of sensors 11 to 15, which in many cases failed for the test runs.

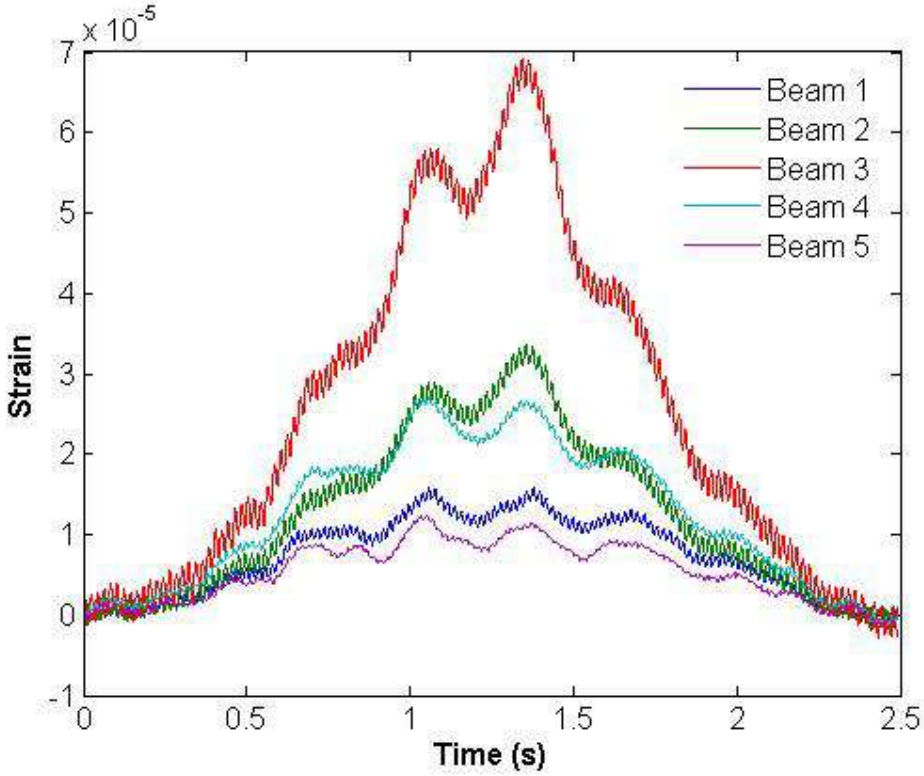

(a)– Unfiltered strain recorded at mid-span

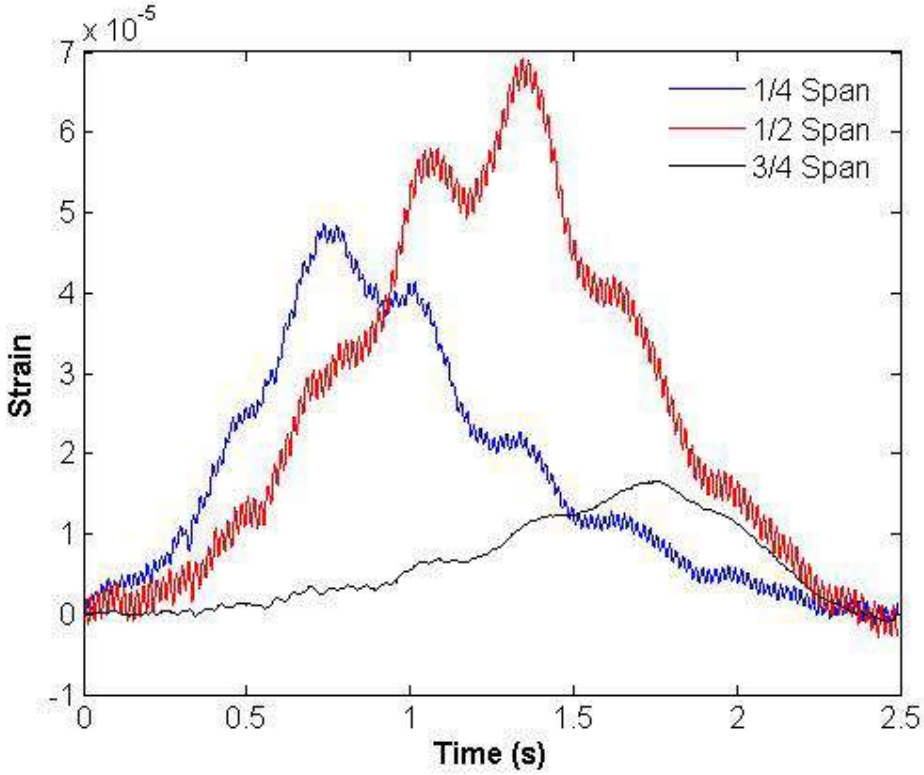

(b) - Unfiltered strain recorded at beam 3

Figure 7.13 – Unfiltered strain recorded due to the 3-axle vehicle travelling in lane 1 at 11.65 m/s

8.6 Finite Element Modelling of Vransko Bridge

The 2d moving force identification algorithm of the previous chapter requires a finite element model of the bridge, which accurately represents the measured frequencies. The finite element model of the bridge in Matlab, utilises the plate element defined in chapter 6 to model the deck, and grillage members to model the additional stiffness provide by longitudinal and diaphragm beams.

8.6.1 Bridge Geometry and Mesh Discretisation

The bridge is of beam and slab construction with diaphragm beams across the supports. The geometry utilised for the finite element modelling is taken from the plans and is shown in figure 8.14

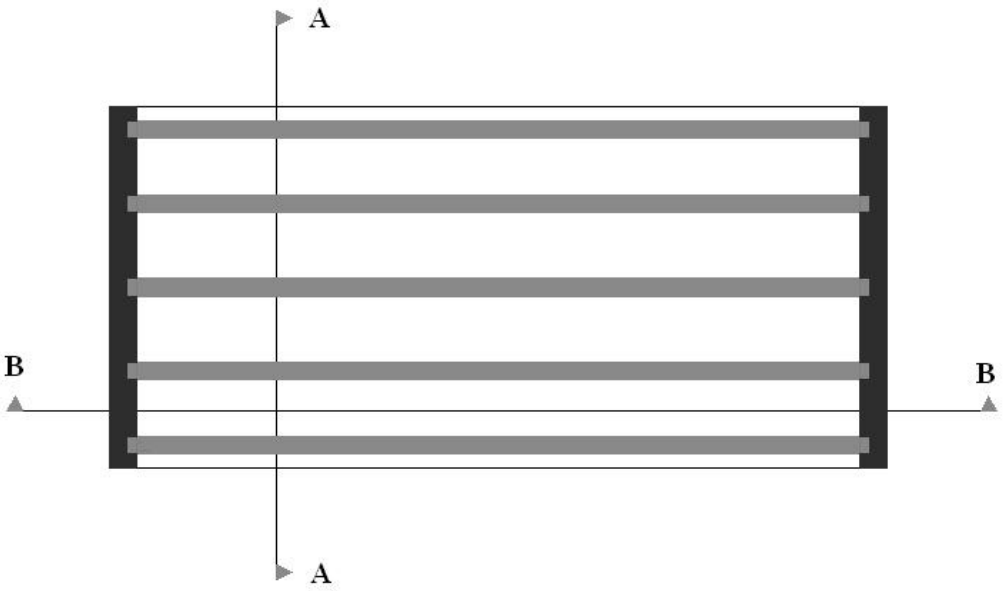

(a) – Bridge Plan

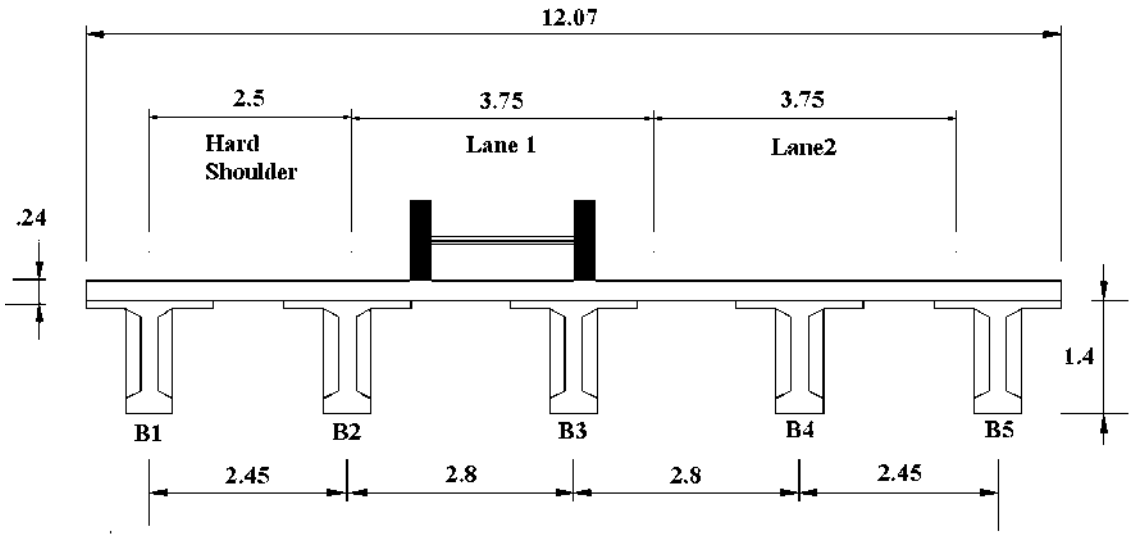

(b) – Section A-A

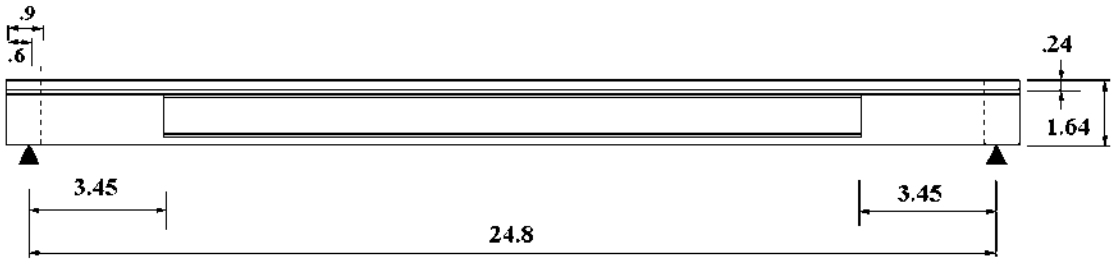

(c) – Section B-B

Figure 8.14 – Bridge geometry

The deck is meshed using the plate element from chapter 6. However it is clear from figure 8.14 that the spacing between the five beams will govern the initial geometry of the mesh. In the transverse direction the deck is discretized between beams. The mesh geometry of the deck in the transverse direction is shown in figure 8.15 and figure 8.16 shows an isometric view of the slab model. The total number of elements used in the transverse direction is 20, the average size for an element is 0.6 m and the depth of the deck from the drawings is 0.24 m.

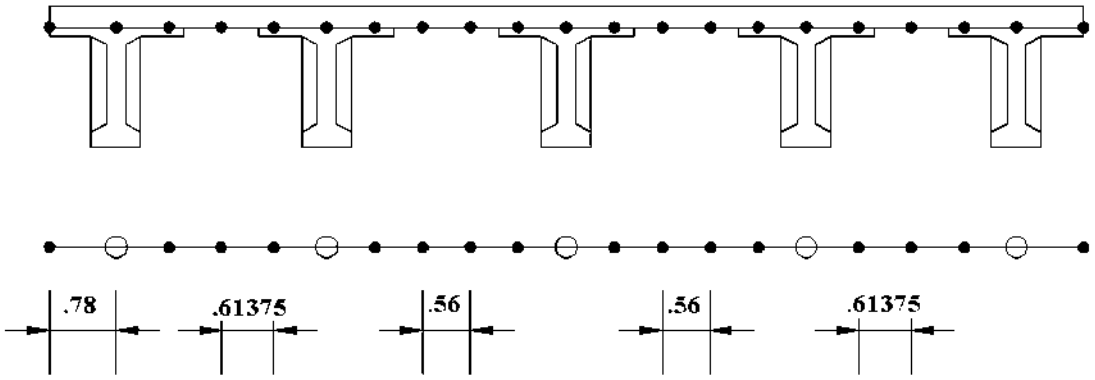

Figure 8.15 – Mesh discretisation in transverse direction

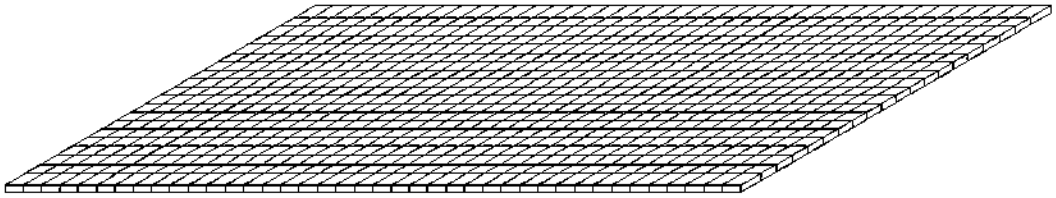

Figure 8.16 – Isometric view of bridge deck

Both the longitudinal and transverse beam members are modelled using two noded beam elements with three degrees of freedom per node, one translation and two rotations. The stiffness matrix for a beam element with a total of six degrees of freedom is defined in equation (8.1) (Logan 1992, Przemieniecki 1968). The mass matrix for the plate contains entries for both the consistent mass matrix, and the mass matrix for rotary inertia. For completeness the mass matrix with rotary inertia for the beam element is used in the generation of the global mass matrix. The complete mass matrix for a 6-degree of freedom element containing entries for both the rotary and torsional inertia of the element is defined by (Przemieniecki 1968) in equation (8.2).

$$K_e = \begin{bmatrix} \frac{12EI}{L^3} & 0 & \frac{6EI}{L^2} & -\frac{12EI}{L^3} & 0 & \frac{6EI}{L^2} \\ 0 & \frac{GJ}{L} & 0 & 0 & -\frac{GJ}{L} & 0 \\ \frac{6EI}{L^2} & 0 & \frac{4EI}{L} & -\frac{6EI}{L^2} & 0 & \frac{2EI}{L} \\ -\frac{12EI}{L^3} & 0 & -\frac{6EI}{L^2} & \frac{12EI}{L^3} & 0 & -\frac{6EI}{L^2} \\ 0 & -\frac{GJ}{L} & 0 & 0 & \frac{GJ}{L} & 0 \\ \frac{6EI}{L^2} & 0 & \frac{2EI}{L} & -\frac{6EI}{L^2} & 0 & \frac{4EI}{L} \end{bmatrix} \tag{8.1}$$

$$M_e = \rho AL \begin{bmatrix} \frac{13}{35}+\frac{6I_y}{5AL^2} & 0 & \frac{11L}{210}+\frac{I_y}{10AL} & \frac{9}{70}-\frac{6I_y}{5AL^2} & 0 & -\frac{13L}{420}+\frac{I_y}{10AL} \\ 0 & \frac{J_x}{3A} & 0 & 0 & \frac{J_x}{6A} & 0 \\ \frac{11L}{210}+\frac{I_y}{10AL} & 0 & \frac{L^2}{105}+\frac{2I_y}{15A} & \frac{13L}{420}-\frac{I_y}{10AL} & 0 & -\frac{L^2}{140}-\frac{I_y}{30A} \\ \frac{9}{70}-\frac{6I_y}{5AL^2} & 0 & \frac{13L}{420}-\frac{I_y}{10AL} & \frac{13}{35}+\frac{6I_y}{5AL^2} & 0 & -\frac{11L}{210}-\frac{I_y}{10AL} \\ 0 & \frac{J_x}{6A} & 0 & 0 & \frac{J_x}{3A} & 0 \\ -\frac{13L}{420}+\frac{I_y}{10AL} & 0 & -\frac{L^2}{140}-\frac{I_y}{30A} & -\frac{11L}{210}-\frac{I_y}{10AL} & 0 & \frac{L^2}{105}+\frac{2I_y}{15A} \end{bmatrix} \tag{8.2}$$

For the longitudinal grillage members, the properties of the combined beam and the width of slab above it, are calculated relative to the centroidal axis of the combined section (O'Brien & Keogh 1999). The equivalent properties of the beam were then calculated from the combined section, minus the properties of the deck about its own axis. The cross section used in the finite element modelling of the beams is identical to that of the drawings. Figure 8.17 shows the beam element and the cross-sections used in the finite element modelling. The torsional constant for the square cross-sections was calculated from empirical formulas (O'Brien & Keogh 1999, Ghali and Neville 1997); for irregular cross-sections the torsional constant was estimated by summing the individual torsional constants of the equivalent rectangular cross sections (O'Brien & Keogh 1999, Chen 1999).

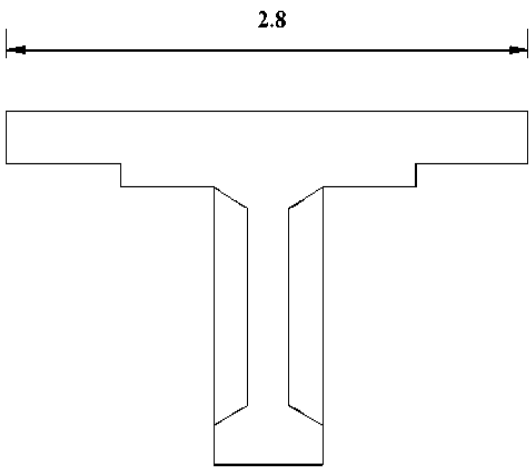

(a) – Equivalent cross section for beam 3

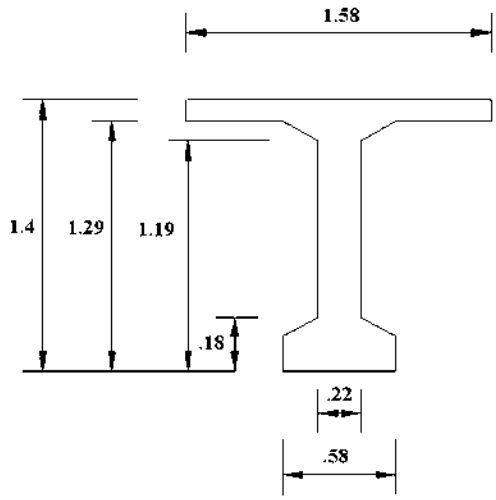

(b) – Schematic 1 of longitudinal beam in the central region

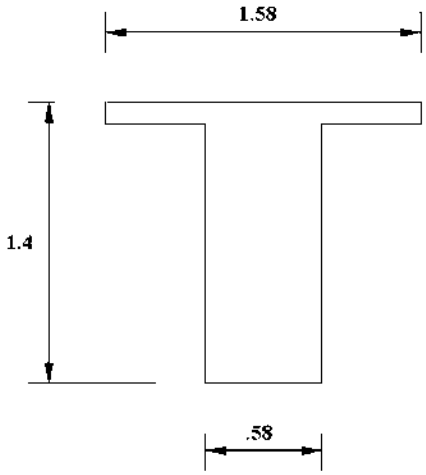

(c) – Schematic 2 of longitudinal beam near to the supports

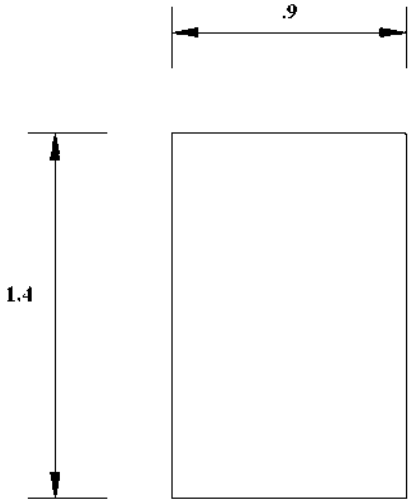

(d) – Schematic of diaphragm beam

Figure 8.17 – Cross-sections of beams used in finite element modelling

The slab, longitudinal and transverse beams are discretized and meshed using programs developed in Matlab. In total the bridge is discretised into 800 plate elements and 236 beam elements with a total of 861 nodes and 3444 degrees of freedom. Figure 8.18 shows the finite element model with both the plate and beam elements, and figure 8.19 shows a wire frame representation of the bridge model with the boundary conditions applied.

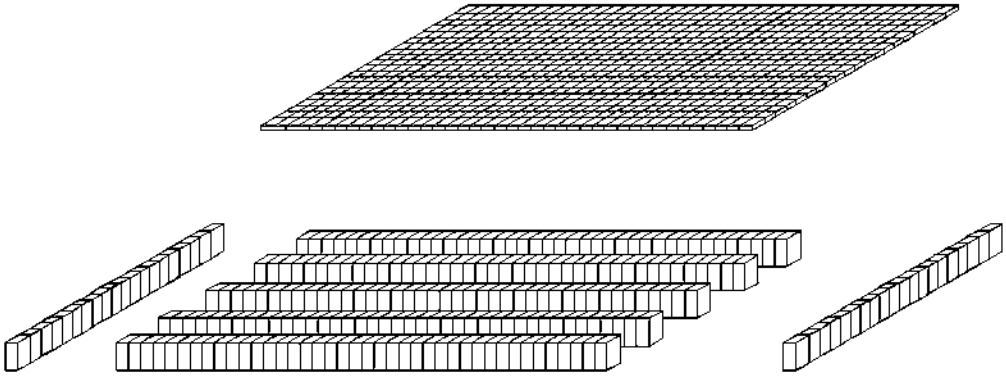

Figure 8.18 – Bridge model with plate and beam elements

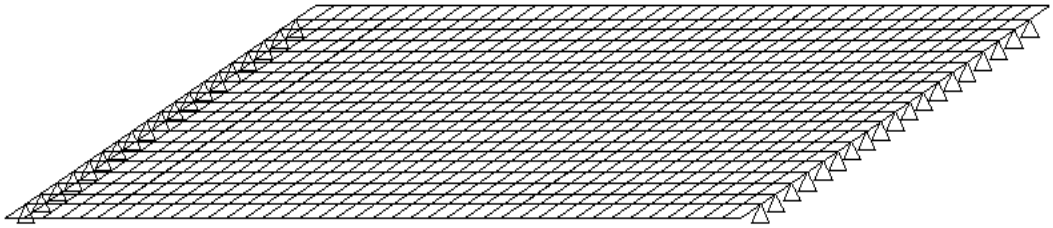

Figure 8.19 – Wire frame representation of the bridge model

8.6.2 Bridge Material

The bridge is of concrete construction; preliminary properties were taken from the engineering drawings, as the material properties are not known. The assumed Young modulus of both the longitudinal and transverse beam members were taken to be 3.4 x 10^{10} N/m^2, with possions ratio of .15 and density of 2400 kg/m^3. The material properties of the slab were not known, the slab was also assumed to be isotropic with material properties equal to those of the beams. It should be noted that these are initial material properties; after testing the model with the measured natural frequencies, the material properties were varied to improve the match.

8.6.3 Modal analysis of the finite element model

From the modal analysis carried out on the experimental data in section 7.4, the first five natural frequencies were found to be 5.11, 6.50, 9.89, 16.12 and 20.55Hz respectively. An eigenvalue analysis was carried out on the Matlab finite element model using the material properties defined in the previous sections; the first five natural frequencies of this model are 4.66, 5.73, 8.79, 15.12 and 18.29Hz. There is a large discrepancy between the natural frequencies of this finite element model and those measured experimentally. The geometry of the bridge is known from both the design drawings and on-site measurements; it is assumed that the density is 2400 kg/m^3. However the exact properties of the concrete beams and the slab are not known. A parametric study of the Young's modulus in the x and y directions of the slab and the beams was carried out, so as to ascertain the optimal Young's moduli which minimise the error in the measured natural frequencies. By sequentially varying the Young's modulus in either the x or y direction, whilst also varying the Young's modulus of the beams, it was found the moduli which minimise the errors in the first five natural frequencies are, E_x = 4.1 x 10^{10} N/m^2 and E_y = 3 x 10^{10} N/m^2 for the deck, and E_b = 3.5 x 10^{10} N/m^2 for the longitudinal and transverse beams. The first 5 natural frequencies for the measured, initial and final FE models are represented in table 8.3 and graphically in figure 8.20. The difference between the measured and predicted natural frequencies for both the initial and final FE models are also represented in table 8.3 and figure 8.21.

Measured (Hz)	Preliminary Properties (Hz)	% Error	Final Properties	% Error
5.11	4.66	8.8	4.94	3.1
6.50	5.73	11.8	6.47	0.3
9.89	8.79	11.1	9.92	-0.3
16.12	15.12	6.2	16.16	-0.2
20.55	18.29	10.9	19.41	5.5

Table 8.3 – First five natural frequencies of FE model

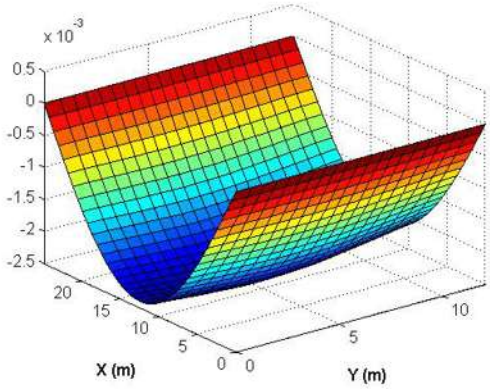

(a) – 1st mode 4.94Hz

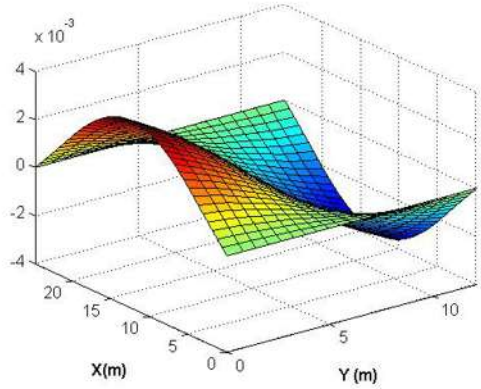

(b) – 2nd mode 6.47Hz

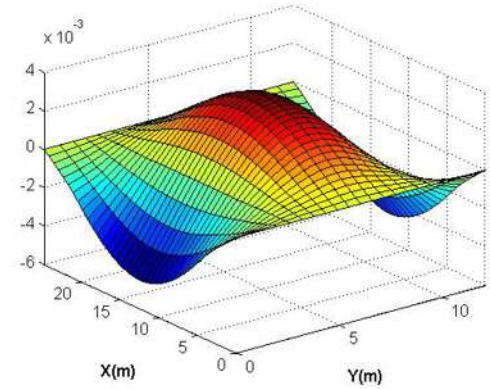

(c) – 3rd mode 9.92Hz

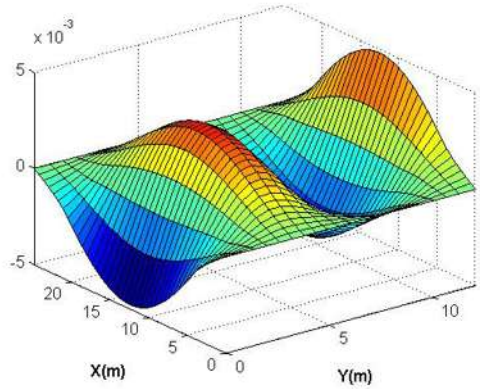

(d) – 16.16Hz

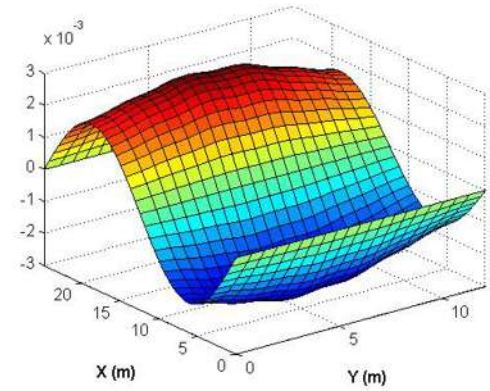

(e) – 19.41Hz

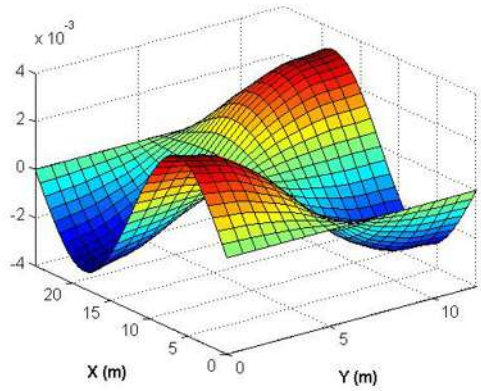

(f) – 21.36Hz

Figures 8.20 – First six modes of vibration of Vransko Bridge.

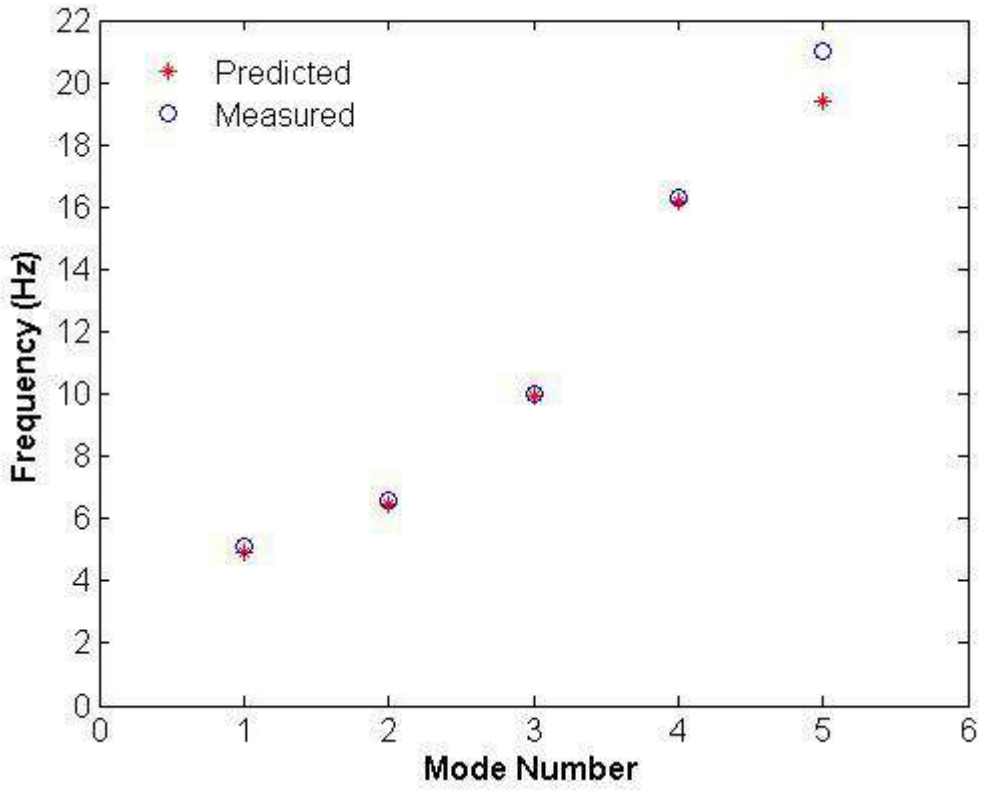

Figure 8.21 – Measured and predicted frequencies of the Vransko bridge

8.6.4 Numerical Simulation of the Test Truck

The revised finite element model of the Vransko Bridge exhibits a good correlation between the measured natural frequencies and those predicted from the eigenvalue analysis. However it is also necessary to compare the results from the experimentally recorded strain data with those of the finite element model. Unfortunately, as no static testing was carried out on site, it is necessary to perform a dynamic comparison of the strain sensors results. The finite element model of the bridge is simulated for the scenario of the test vehicle described in section 8.5, idealised as six constant loads equal in magnitude to the static axle weights of the truck. The recorded strain for the test vehicle travelling in lane 1 of the bridge at 11.9 m/s, is compared with the simulated strain from the finite element model. Figure 8.22 shows the comparison between the experimentally measured strain on the third beam at quarter span and mid-span. As can be seen from this figure, there is a reasonably good match between the experimentally measured and the simulated data. It can be seen that both the magnitude and the shape of the response are of a similar magnitude. However there is a frequency in the

measured strain that is not present in the simulated. This frequency is approximately 3Hz, which is not the first measured natural frequency of the bridge. It is thought that this frequency corresponds to one of the trucks natural frequencies; this could indicate that the dynamic response of the bridge is predominately due to the truck.

Figure 8.23 shows a comparison between the experimentally recorded and the simulated strain for all of the sensors at mid span. As can be seen, the match between the simulated and the measured data from beams 1, 2, 4 and 5 is poor. Although the shape of the response appears to be correct, there is a significant error in the magnitude. There are various reasons for these large errors between the signals. The amplification of the strain sensors could be incorrect; the sensors may not be correctly calibrated. The finite element model employed may not be complex enough to accurately model the transverse behaviour of the bridge and the correct distribution of the vehicle forces.

However the most likely reasons for the inaccuracies in the transverse behaviour of the bridge are, that the assumed locations of the truck and wheels are not correct and/or poor modelling of the transmission of forces locally down to the beam. The assumed behaviour of the beam and slab model is that the wheel loads are distributed to the beams through a bending action. This may not be true; a significant proportion of the wheel load could be distributed to the beams via compression instead of a bending action. Finally there could be an arching effect (Bakht & Jaeger 1985) in the transverse direction of the slab, which has not been accounted for in the FE model.

The material properties could again be altered and a comparison made between the simulated and measured data (however this would result in different bridge frequencies). It is also thought that for the MFI algorithm developed in chapter 6, a reasonably accurate dynamic model is required. If the current finite element model and strain transducers 1 to 10 were used in the MFI algorithm, there would be significant errors in the identified forces. This is due to the fact that, although the bridge frequencies are reasonably good, the significant differences in the strain response would result in the MFI algorithm optimising for applied interaction forces that would minimise the difference between the measured and the theoretical, the magnitude of which is significant, therefore inducing large errors in the identified forces. It is

therefore necessary to assess the numerical feasibility of using only 2 sensors in the moving force identification algorithm.

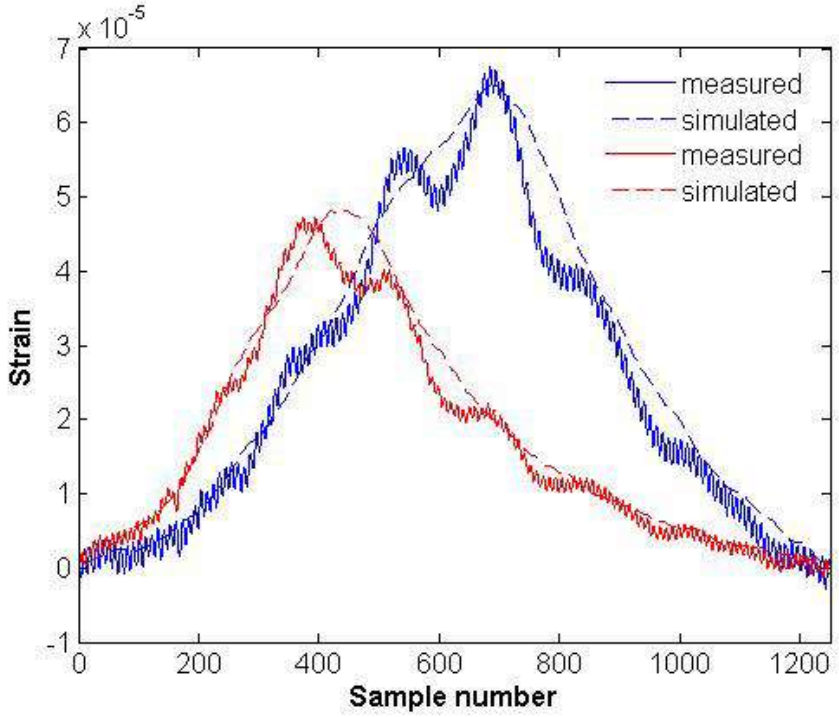

Figure 8.22 – Comparison of the simulated and measured strain at quarter span (red) and mid span (blue) for beam 3, sensors 3 & 8

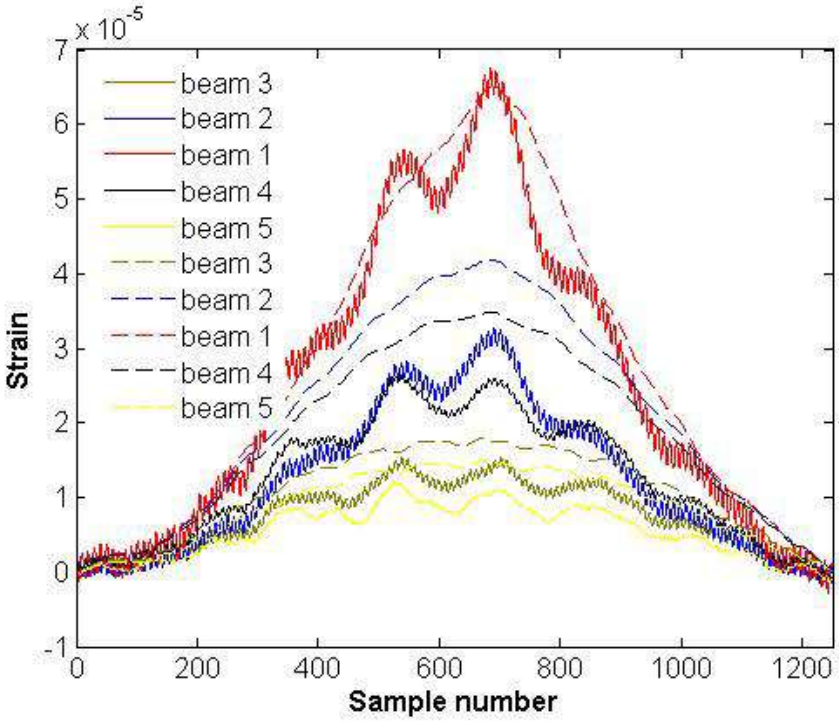

Figure 8.23 – Comparison of the simulated and measured strain at mid span (---- simulated, —— measured)

8.7 Numerical testing of the MFI algorithm using 2 sensors

As stated in the previous section, if only 2 sensors are to be used as the input to the moving force identification algorithm, it is necessary to assess what information can be accurately extracted using only these two sensors. The finite element model of the Vransko Bridge is simulated for the scenario of 6 moving forces defined by,

$$\begin{aligned}
W_1(t) &= 37,200(1+.1\sin(3\pi t)+.1\sin(5\pi t)+.05\sin(25\pi t)+.05\sin(30\pi t)\\
W_2(t) &= 37,200(1+.1\sin(3\pi t)+.1\sin(5\pi t)+.05\sin(25\pi t)-.05\sin(30\pi t)\\
W_3(t) &= 50,000(1-.1\sin(3\pi t)+.1\sin(5\pi t)-.05\sin(25\pi t)-.05\sin(30\pi t)\\
W_4(t) &= 50,000(1-.1\sin(3\pi t)+.1\sin(5\pi t)-.05\sin(25\pi t)+.05\sin(30\pi t)\\
W_5(t) &= 50,000(1-.1\sin(3\pi t)+.1\sin(5\pi t)-.05\sin(25\pi t)-.05\sin(30\pi t)\\
W_6(t) &= 50,000(1-.1\sin(3\pi t)+.1\sin(5\pi t)-.05\sin(25\pi t)+.05\sin(30\pi t)
\end{aligned} \tag{8.3}$$

The static component of the forces is equal to that of the test truck as measured on site. Each wheel of the test truck is contains dynamic components both in phase and out of phase as defined in chapter 7. The moving forces are travelling in lane 1 at 12.76 m/s (see figure 8.14b) with the axle configuration represented in figure 8.12. The simulated strain at quarter and mid span of beam 3, corrupted with 2% gaussian noise, is used as the input to the moving force identification algorithm. From the error analysis carried out in chapter 7, it was found that when 3 sensors are used, it was not possible to identify individual wheel loads; accurate identification is only possible for the individual axle loads. Further to this the MFI algorithm was found to be unable to accurately identify axle forces with axle spacing less than 3m. As the spacing between the back two axles of the test vehicle is 1.38m, the sum of the identified forces for axles 2 and 3 will be used. The optimal regularisation parameter was calculated from the L-curve and the curvature to be approximately 5×10^{-18}. Figure 8.24 shows the predicted versus the applied forces for axle 1, the sum of axles 2 and 3, and the total applied load. It can be seen from the figure that acceptable results using the 2 sensors can be obtained. There is an excellent match between the applied and the identified loads for the total applied load and the sum of the axles 2 and 3. The match between the theoretical force and the predicted for the front axle is not as good. The predicted force does oscillates about the static axle value, but there is only one main frequency predicted and the algorithm fails to predict the higher frequencies. Nevertheless, even

for the case of using only 2 sensors the MFI algorithm still performs reasonably well over all.

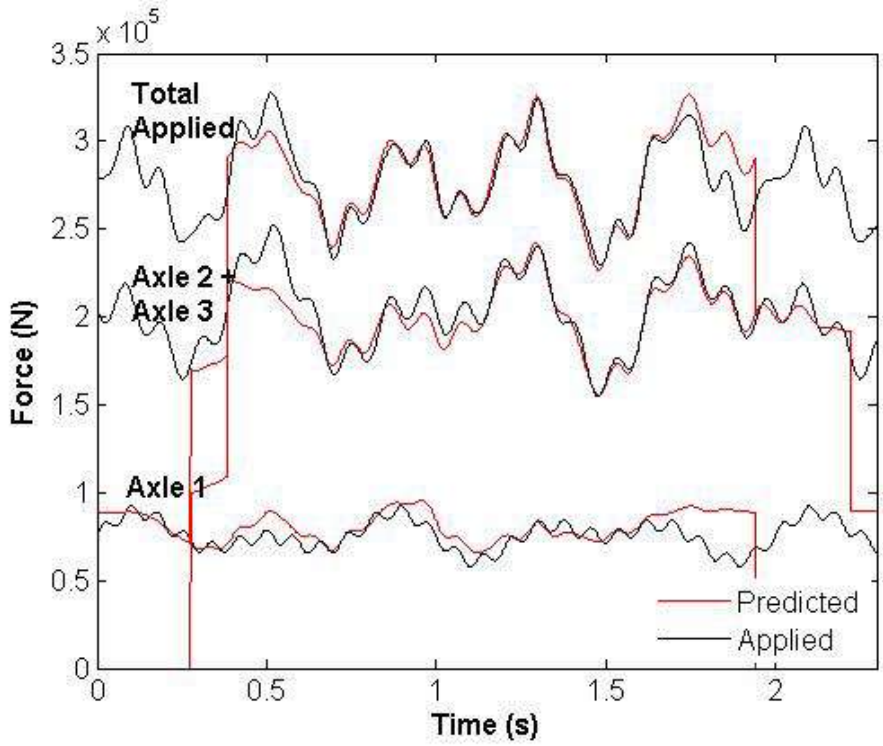

Figure 8.24 – Identified and applied axle forces using 2 sensors

8.8 Moving force identification using field data from the Vransko Bridge

It is not possible to determine the accuracy of the moving force identification algorithm in the field, as the actual applied forces are not known. However, some checks are possible. The axle weights and the gross vehicle weights can be obtained by summing the identified forces in the middle 60% (Chan et al 2000) of the time history for each axle averaging the result, and these can be compared to the known values for the test vehicle. The first natural frequencies can be obtained by carrying out a fast Fourier transform on the time history of the identified forces and the predicted frequencies can then be compared over the range of test runs. The test vehicle is monitored travelling in lane 1 of the bridge at 11.97m/s. The unfiltered raw data has been used for this particular test, the optimal regularisation paramater was calculated from the L-curve, (see figure 8.25a). The regularisation paramater corresponding to the point of maximum

curvature of the L-curve was found to be 2 $\times 10^{-17}$, (see figure 8.25b). The identified force histories using this regularisation paramater are illustrated in figure 8.26. It can be seen that once all of the axles of the vehicle are on the bridge, the dynamic forces oscillate about their static axle weights. The frequency of the applied forces is also distinct in the identified force histories. The frequencies of identified force histories for this event were found from a Fourier analysis to be 2.90 and 3.05 Hz for the front and rear axles respectively.

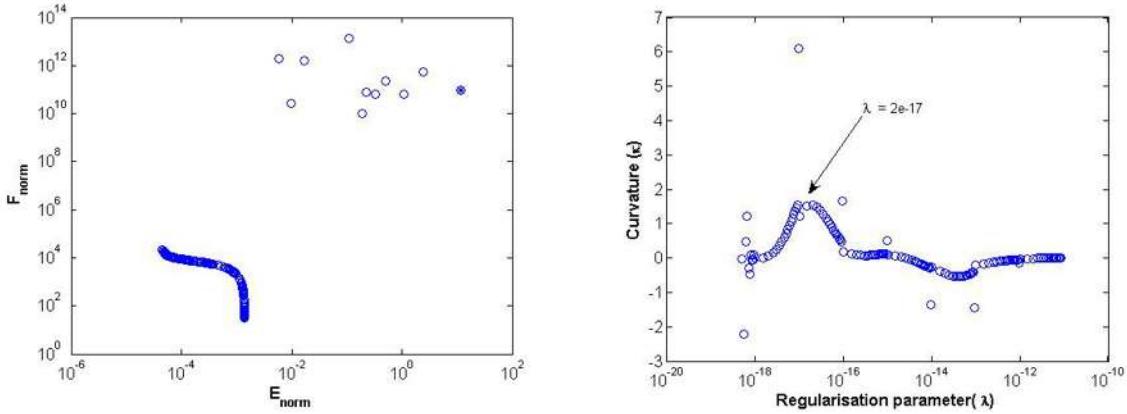

(a) – L-curve **(b)** – Curvature of the L-curve

Figures 8.25 - Optimal regularisation parameter for test truck

The predicted static axle loads for this particular test found from averaging in the middle 60% are, 68.6kN, 203kN and 272kN, for the front axle, the sum of the rear axles and the gross vehicle weight respectively. The represents errors in the predicted axle weights of 7.90%, -1.54% and 1.03% for the front axle, the sum of the rear axles and the gross vehicle weight respectively. The impact factors for the identified force histories, can be defined as the ratio of the maximum applied dynamic force to the static force; the impact factors for this test run were found to be 1.13, 1.16 and 1.10 for the front axle, the rear axles and the total impact factor for the gross weight. The natural frequencies of the truck are calculated by taking a Fast Fourier transform of the identified forces. The identified frequencies were found to be 2.90Hz and 3.05Hz for the front and rear axles, see figure 8.27. These are thought to be reasonable frequencies for a rigid three-axle truck, the frequencies of older steel suspension trucks often ranges between 2.75 and 3.16Hz (Divine 1997).

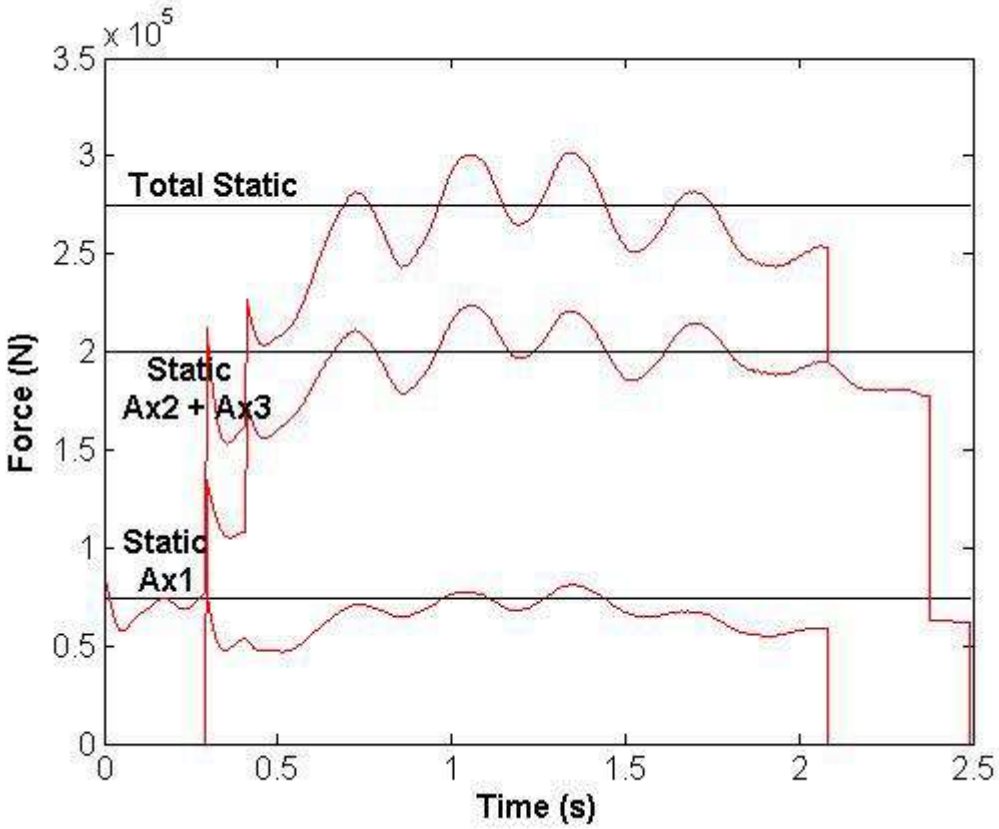

Figure 8.26 – Identified forces for the test vehicle travelling in lane 1, using the unfiltered data

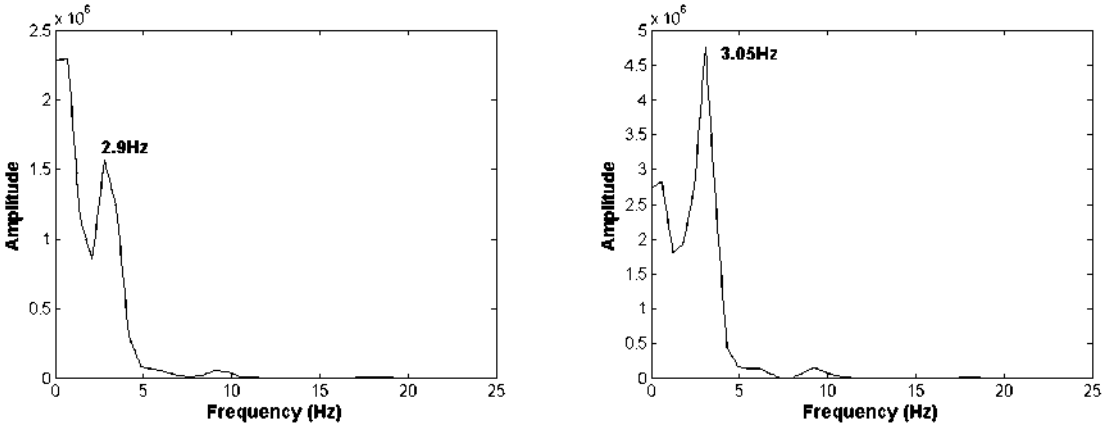

(a) FFT of identified forces axle 1 **(b)** FFT of identified forces axles 2 and 3

Figures 8.27 –Frequency analysis of identified forces

In the previous example the moving force identification was performed using the unfiltered raw data. As only a few of the test runs contained both the raw and digitally filtered data, it is useful to make a comparison between the identified forces using both sets of data. Figure 8.28 shows the identified forces using the filtered and unfiltered strain data for the test vehicle travelling in lane 1 at 11.97 m/s, it can be seen from this

figure that the identified forces in both cases are almost identical, the only significant difference is that the optimal regularisation paramater using the filtered data has reduced to 5×10^{-18}.

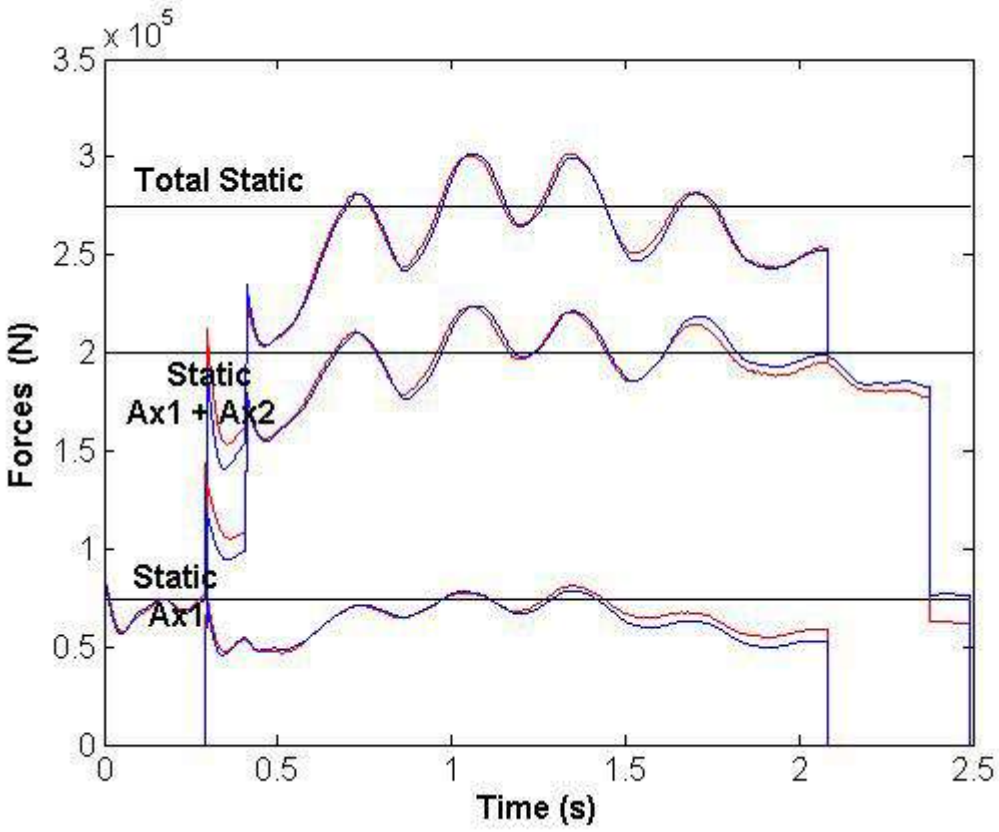

Figure 8.28 - Identified forces for the test vehicle travelling in lane 1 at 11.97 m/s, using the unfiltered data (red) and the filtered data (blue).

Figure 8.29 shows the identified forces for the vehicle travelling in lane 1 at 11.63 m/s. Again it is clear from this figure that the identified axle forces oscillate about the static axle weights in a similar manner to those identified using the raw data at a similar velocity. Again the frequency of the test vehicle is distinct in the identified forces. The impact factors using the digitally filtered data were calculated to be 1.30, 1.08 and 1.07 for the front axle, the rear axles and the total impact factor for the total applied load. The frequencies of the front and rear axles were calculated to be approximately 3.0 Hz and 3.3Hz respectively.

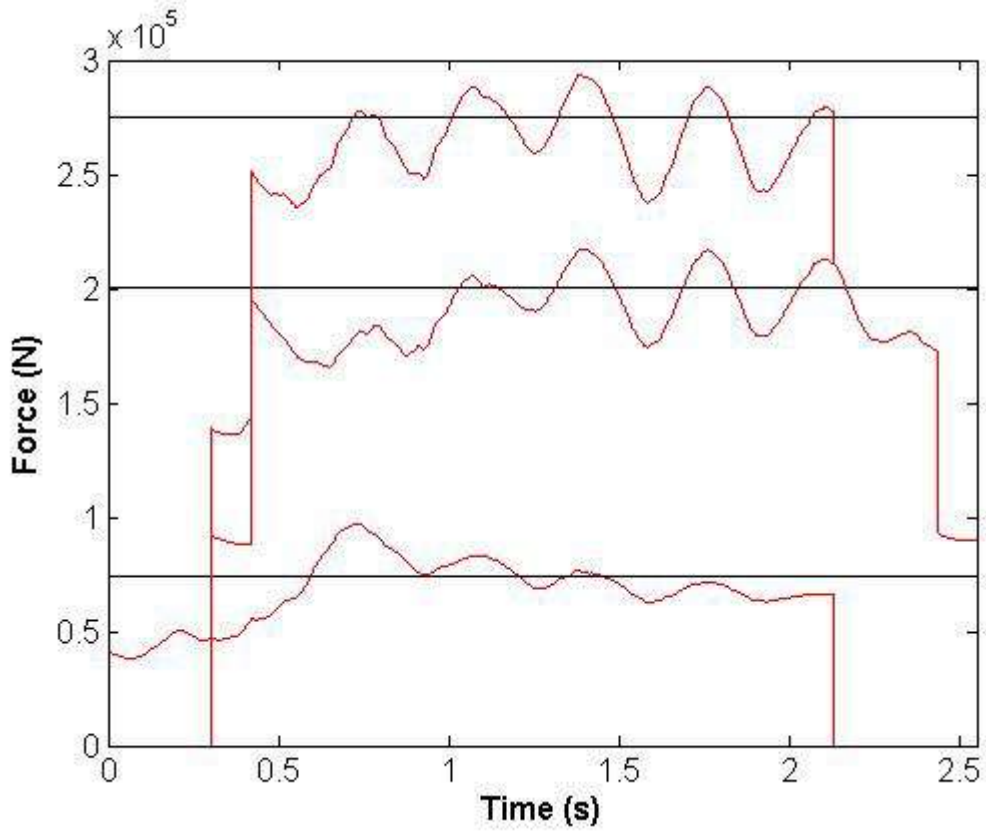

Figure 8.29 – Identified axle forces using the digitally filtered data

A total of 14 single runs were made, with the calibration truck travelling in lane 1 of the bridge. Due to multiple vehicle presence (i.e., other traffic) on the bridge the number of runs that could be used for testing the MFI algorithm was reduced to 9. Figure 8.30 shows the identified forces for some of the 9 single vehicle events with the test vehicle travelling in lane 1. It is clear from this figure 8.30 that the identified forces in general oscillate about the static axle loads of the vehicle with a similar frequency for each run. However it should be noted that for the first axle of the test vehicle, the identified forces at the start of the bridge are always less than the static axle load. It is only over the period when all three axles are on the bridge that the identified forces for the first axle oscillates about the static axle value. It is therefore recommended that the time period for which only one axle is present on the bridge be ignored when calculating the solution.

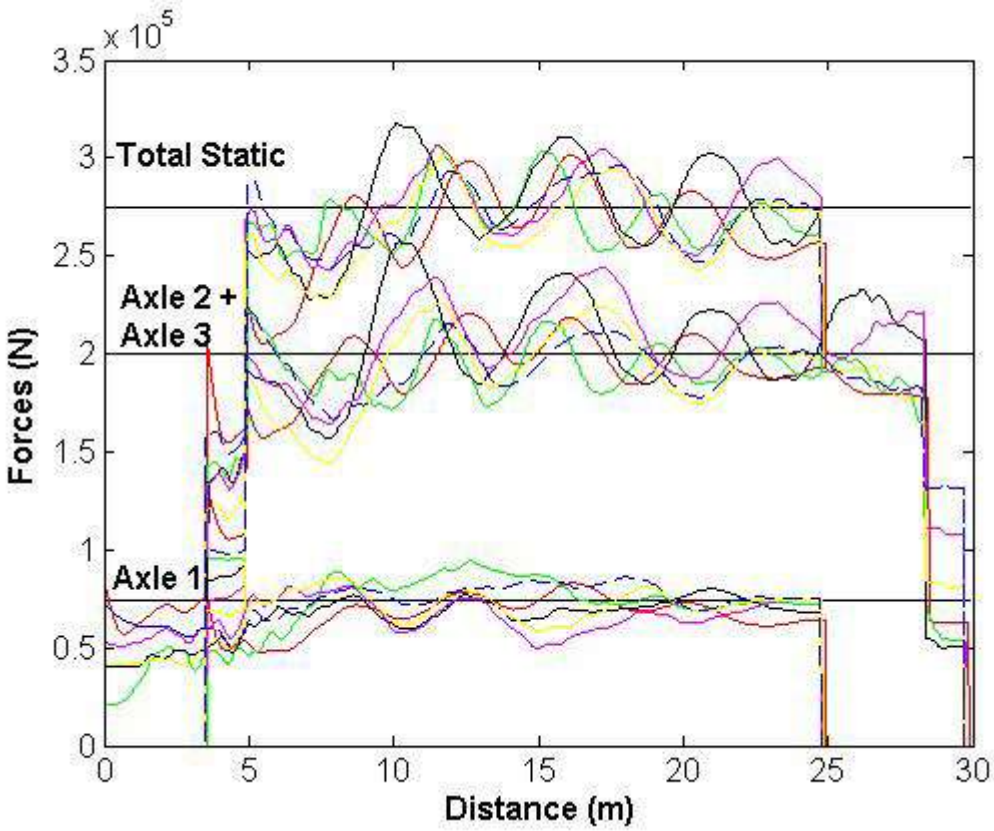

Figure 8.30 – Identified axle forces versus distance

For all of the test runs, the static axle and gross vehicle weights were calculated from the central 60% of the identified force time histories. Table 8.4 shows the percentage errors for the predicted static weights for each of the runs. In general the percentage error in the static axle weights and the GVW is reasonable, with a maximum error in GVW of 3.8% and a max error for axles 2 and 3 of 6.9%. The percentage error in the static weights of axle 1 are again generally reasonable. However, there is one event for the vehicle travelling at 11.34 m/s where the error is 17%. For this particular run the error in axles 2 and 3 is 6.9%, the highest encountered in the rear axles as well, whilst the error in the gross vehicle is only 0.3%. This equates to an under estimation of the front axle and an over estimation of the rear axles, this could be due to an error in the calculated vehicle velocity.

In each of the test runs, the impact factors for the front, rear and total force were calculated. Table 8.5 show the impact factors for each of the test runs. The maximum impact factors calculated are 1.35, 1.28 and 1.27 for the front, rear and total loads respectively. The only conclusive trend observed is that the impact factors for the front

axle are bound between 1.1 and 1.35, and for the rear axles are bound by 1.08 and 1.28. Figure 8.31 shows the identified forces for the event in which the maximum impact factor occurs for the rear axles.

Table 8.6 shows the frequencies of the identified force histories for the front and rear axles of the test vehicle for all of the test vehicle events. The average frequencies for the front and rear axles are 3.2Hz and 3.12Hz respectively. This compares very well with the frequencies suggested by the OECD Divine programme (Divine 1997), which suggests frequencies between 2.75 and 3.2Hz for steel suspension systems in North America and Europe.

% Error			Velocity
Axle 1	**Axle 2+3**	**GVW**	**(m/s)**
7.9	-1.5	1.0	11.97
-2.0	5.0	3.0	11.63
-17.4	6.9	0.3	11.31
-3.9	3.4	1.4	10.55
10.8	-2.7	0.9	13.93
5.0	-0.5	0.9	14.84
9.5	-4.0	-0.3	18.45
3.2	4.0	3.8	19.14
-1.7	2.8	1.5	19.50

Table 8.4 – Percentage error in the static axle weights of the test vehicle

Velocity	Impact Factor		
(m/s)	**Axle 1**	**Axle 2+3**	**Total**
11.97	1.13	1.12	1.09
11.63	1.30	1.08	1.07
11.31	1.34	1.08	1.12
10.55	1.26	1.09	1.12
13.93	1.03	1.14	1.09
14.84	1.08	1.28	1.16
18.45	1.09	1.22	1.27
19.14	1.15	1.13	1.10
19.50	1.15	1.12	1.08

Table 8.5 – Impact factor for the identified forces

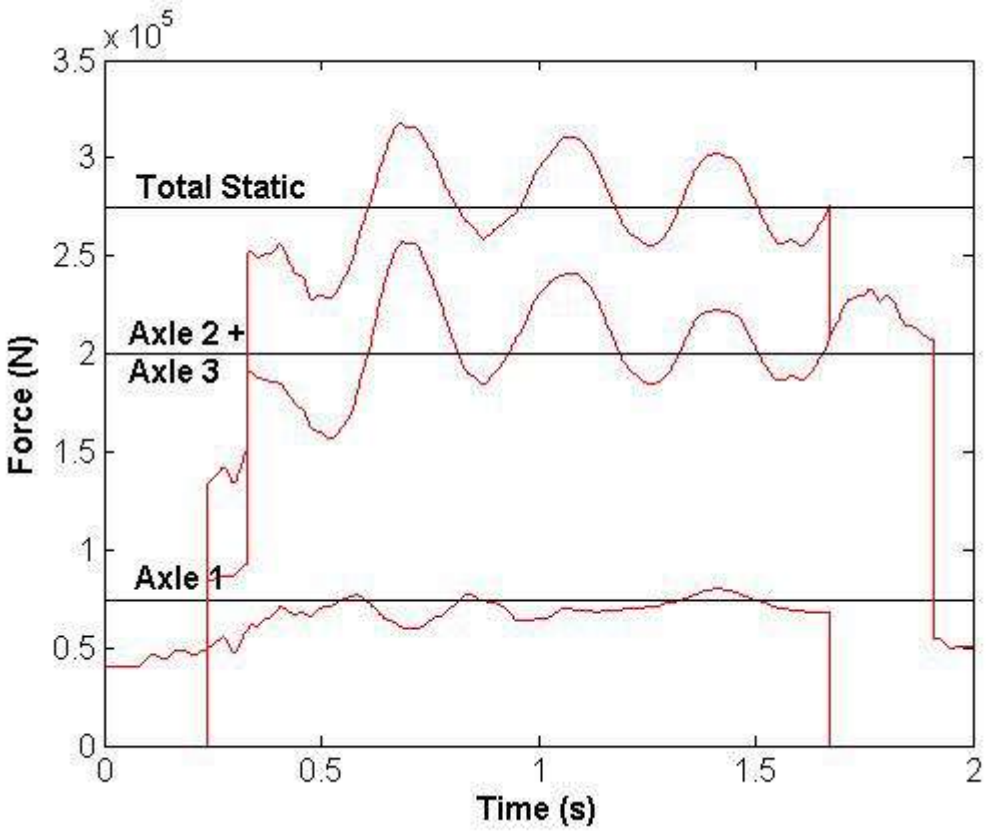

Figure 8.31 – Identified forces for the test vehicle travelling at 14.84m/s

Velocity (m/s)	Axle 1 (Hz)	Axle 2+3 (Hz)
11.97	2.9	3.1
11.63	3.0	3.3
11.31	3.1	3.0
10.55	3.3	3.0
13.93	3.0	3.0
14.84	3.0	2.7
18.45	3.0	3.0
19.14	3.7	3.4
19.50	3.8	3.7

Table 8.6 – Frequencies of the identified forces

8.9 Conclusions

The 2d moving force identification algorithm of chapter 6 has been experimentally validated in the field in collaboration with ZAG. The experimental programme carried out in Slovenia has been outlined. The installation of the strain transducers and the axle detectors has been detailed along with details of the data acquired. The frequency analysis of the measured strain data has been presented, along with the measured natural frequencies. Details of the finite element model used for the inverse analysis have been presented. The finite element modelling was modified from that of chapter 6 by the addition of the grillage beam members to model the longitudinal and diaphragm beams. The finite element model has been validated with the measured frequencies in the field. There was found to be poor correlation between some of the strain transducers and the simulated strain from the FE model. The test set-up is not ideal, and for proper calibration of an FE model both dynamically and statically, significant improvements to the identified results could be made using the results from static testing of the bridge, to correctly calibrate the strain sensors. In fact adopting a testing program where both static testing is carried out in conjunction with more accurate dynamic testing where the actual mode shapes of the bridge are measured using accelerometers (Chan 2000, Li 2005 a & b) would be ideal. It is thought that a testing program of this nature would result in a more accurate finite element model that not only represents the dynamic properties but also the static behaviour of the bridge. It is thought that this would result in more sensors being used in the inverse analysis and hence more information on the dynamic loads, even information on the imparted wheel loads could be identified.

Notwithstanding this the viability of using only two sensors has been justified numerically first, and it has been shown that valuable information of the truck dynamics can be identified using only two sensors. Finally the moving forces imparted by the truck to the road surface on the bridge have been identified over a range of velocities, and in all cases the oscillation of the truck forces about the static axle weight is distinct. Information has been inferred on the frequencies of the forces, which is likely one of the truck's natural frequencies. Finally the impact factors over a range of velocities have been calculated for the test truck.